A PDE-DDE MODEL FOR CELL POLARIZATION
IN FISSION YEAST[*]

BIN XU[†] AND PAUL C. BRESSLOFF[†]

Abstract. We consider a one-dimensional model of cell polarization in fission yeast consisting of a hybrid partial differential equation–delay differential equation system. The model describes bulk diffusion of the signaling molecule Rho GTPase Cdc42 in the cytoplasm, which is coupled to a pair of delay differential equations at the ends of the cell via boundary conditions. The latter represent the binding of Cdc42 to the cell membrane and rerelease into the cytoplasm via unbinding. The nontrivial nature of the dynamics arises from the fact that both the binding and unbinding rates at each end are taken to depend on the local membrane concentration of Cdc42. In particular, the association rate is regulated by positive feedback and the dissociation rate is regulated by delayed negative feedback. We use linear stability analysis and numerical simulations to investigate the onset of limit cycle oscillations at the end compartments for a cell of fixed length, distinguishing between symmetric solutions in which the mean concentration is identical at both ends and asymmetric solutions where the mean concentration at one end dominates. We find that the critical time delay for the onset of oscillations via a Hopf bifurcation increases as the diffusion coefficient D decreases. We then solve the diffusion equation on a growing domain under the additional assumption that the total amount C_{tot} of the signaling molecule increases as the cell length increases. We show that the system undergoes a transition from asymmetric to symmetric oscillations as the cell grows, consistent with experimental findings of "new-end-take-off" in fission yeast. (The latter refers to the switch from monopolar to bipolar growth as the cell grows.) The critical length where the switch occurs depends on D and the growth rate.

Key words. cell polarization, fission yeast, diffusion, delay differential equations, Hopf bifurcation

AMS subject classifications. 92C15, 92C42, 35K57

DOI. 10.1137/16M1065458

1. Introduction. In this paper, we analyze a novel diffusion type problem with active boundary compartments relevant to the triggering or nucleation of actin during cell polarization of fission yeast *Schizosaccharomyces pombe*. Fission yeast is a rod-shaped cell consisting of two hemispheres of constant radius that cap a cylinder of increasing length. Thus growth is effectively one-dimensional (1D) (axial). There are distinct stages of cell growth that are regulated by the cell cycle, as illustrated in Figure 1. Immediately following cell division, the cell initially grows at one end only, namely, the "old end" of the previous cell cycle (monopolar growth). However, during the G2 phase of the cell cycle, the cell also starts growing from the new end (bipolar growth), in a process known as "new-end-take-off" (NETO) [13, 6, 9]. Cell growth then ceases during mitosis, after which the cytoskeletal growth machinery is directed toward the division site for cell separation.

Recent experimental evidence suggests that the signaling molecule Rho GTPase Cdc42 plays an important role in regulating polarized growth in fission yeast [8]. Labeling active Cdc42 within fission yeast cells using a fluorescent marker, Das et al. [8] observed Cdc42 oscillations with an average period of 5 min. The oscillations

[†]Department of Mathematics, University of Utah, Salt Lake City, UT 84112 (xu@math.utah.edu, bressloff@math.utah.edu).
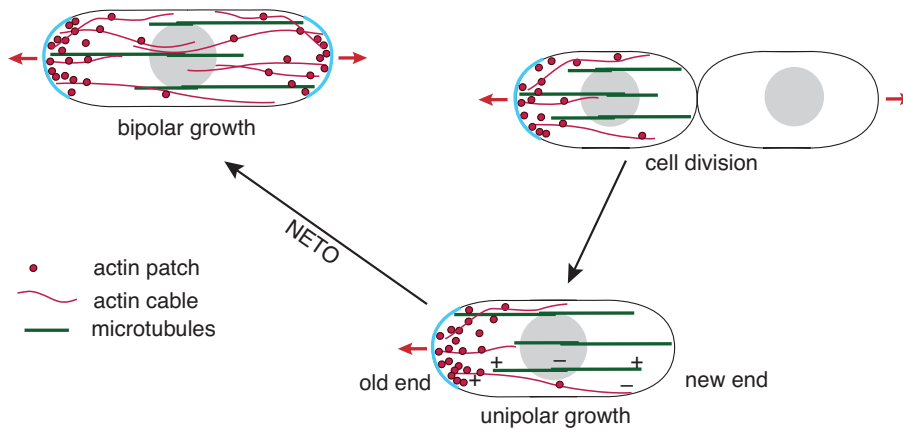
FIG. 1. *Cytoskeleton organization of fission yeast during the cell cycle. Sites of active growth are labeled by the red lines and arrows. The microtubules (green), actin cytoskeleton (dark red), and protein-rich membrane domains (light blue) are depicted at representative cell cycle stages. The microtubules form cytoskeletal tracks for molecular motors to transport landmark proteins to the cell tips, which then regulate cell growth via the nucleation and polymerization of actin. There are two main types of actin structure involved in the polarized growth of yeast cells: cables and patches. Actin patches consist of networks of branched actin filaments nucleated at the plasma membrane, whereas actin cables consist of long, unbranched bundles of actin filaments. Myosin motors travel along the cables unidirectionally toward the actin barbed ends at the plasma membrane, transporting intracellular cargo such as vesicles, mRNA, and organelles necessary for growth. The actin patches act to recycle membrane bound structures to the cytoplasm via endocytosis.*

occurred at both tips and were out-of-phase (anticorrelated). In the case of longer cells exhibiting bipolar growth, the mean amplitude of the oscillations were the same at both ends (symmetric, anticorrelated oscillations). On the other hand, for shorter, less mature cells exhibiting monopolar growth, the amplitude was significantly larger at the growing end (asymmetric, anticorrelated oscillations). The observed dynamics suggests that there is competition for active Cdc42 (or associated regulators) at the two ends and indicates the presence of some form of delayed feedback. This motivated Das et al. [8] to model Cdc42 oscillations in terms of a system of delayed differential equations (DDEs) with positive feedback and delayed negative feedback. The DDE model was able to account for the transition from oscillating monopolar (asymmetric) to oscillating bipolar (symmetric) states during cell elongation. However, one of the potential limitations of the Das et al. model is that the effects of cytosolic diffusion were ignored. That is, the concentration of Cdc42 in the bulk of the cell was assumed to be spatially uniform and could thus be determined by imposing conservation of total Cdc42 within the cell at a given length.

We extend the Das et al. model in order to investigate the effects of cytosolic bulk diffusion and cell length on Cdc42 oscillations. Exploiting the rod-like geometry of fission yeast, we treat the cell as a finite 1D domain of length L. Cdc42 diffuses within the interior of the domain, $x \in (0, L)$, and can bind to the cell membrane at the ends $x = 0, L$. Moreover, membrane-bound Cdc42 can unbind and reenter the cytosol. The nontrivial nature of the dynamics arises from the fact that both the binding and unbinding rates at each end are taken to depend nonlinearly on the local membrane concentration. In particular, the association rate is regulated by positive feedback and the dissociation rate is regulated by delayed negative feedback along lines identical to the model of Das et al. [8]. The resulting dynamical system takes

the form of a coupled PDE-DDE, where the bulk dynamics is described by a simple diffusion PDE, and the exchange of Cdc42 between the cytolsol and the end membrane compartments is modeled in terms of flux boundary conditions that involve both the positive and delayed negative feedback (DDE).

From a mathematical perspective, our model is a new example of a class of models recently formulated and studied by Gou, Ward, and collaborators [10, 11]. These consist of spatially segregated dynamically active units, such as cells or localized signaling compartments, that are coupled with each other via a signaling molecule that diffuses in the bulk domain between the active units. Gou et al. [10, 11] considered the particular case in which each isolated compartment is a conditional oscillator. That is, in isolation a compartment's dynamics is at a stable fixed point but can exhibit sustained oscillations in a different parameter regime. For the sake of illustration, each isolated compartment was modeled in terms of a planar dynamical system (without delays). Using linear stability analysis, the authors showed that diffusive coupling can induce in-phase or antiphase oscillations for a pair of active compartments. There are, however, a number of differences between our model and those studied by Gou et al. [10, 11]. First, our membrane compartments are not conditional oscillators, that is, the existence of oscillations depends crucially on the delayed coupling between the compartments and the bulk diffusion. Second, there is only one chemical species in our model, that is, the signaling molecule is the same molecule as in each active compartment. Third, the size of the domain changes during cell elongation.

The structure of the paper is as follows. In section 2, we introduce our PDE-DDE model for Cdc42 oscillations in fission yeast. In section 3, we show that our model reduces to the DDE model of Das et al. [8] in the fast diffusion limit. In order to provide a baseline for comparisons with the full model, we investigate conditions for a Hopf bifurcation using a mixture of numerical simulations and linear stability analysis. (Note that this was not carried out by Das et al.) We then turn to the analysis of the full PDE-DDE model in section 4. One major result of our work is to demonstrate that for biophysical values of diffusivity, bulk diffusion can have a significant effect on the critical time delay and amplitude of Cdc42 oscillations for a cell of fixed length. We then solve the diffusion equation on a growing domain under the additional assumption that the total amount C_{tot} of the signaling molecule increases as the cell length increases. We show that the system undergoes a transition from asymmetric to symmetric oscillations as the cell grows, consistent with experimental findings of "new-end-take-off" in fission yeast. We also show that the critical length where the switch occurs depends on both D and the growth rate.

2. The PDE-DDE model. Consider a 1D compartmental model consisting of a PDE for the substrate concentration in the cytosol and a DDE for the concentration at each end compartment; see Figure 2. The length of the domain is taken to be L. Let $C(x,t)$ be the cytosolic concentration of Cdc42 at x and $X_i(t)$, $i = 1, 2$, the concentration of Cdc42 at the ith compartment, where $t, t > 0$, denotes time. (Concentrations are defined as the number of molecules per unit cross section of the cell, which is assumed to be fixed.) The PDE-DDE model is taken to be

$$(2.1a) \qquad \frac{\partial C(x,t)}{\partial t} = D \frac{\partial^2 C(x,t)}{\partial x^2}, \quad 0 < x < L, \quad t > 0,$$
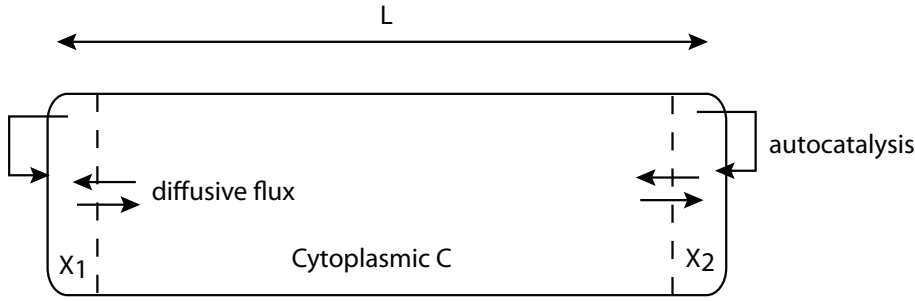
FIG. 2. *Compartmental model of NETO based on Cdc42 oscillations.*

with flux boundary conditions

(2.1b) $\qquad -D\partial_x C(0,t) = -k^+(X_1(t))C(0,t) + k^-(X_1(t), X_1(t-\tau))X_1(t),$

(2.1c) $\qquad -D\partial_x C(L,t) = k^+(X_2(t))C(L,t) - k^-(X_2(t), X_2(t-\tau))X_2(t),$

and

(2.1d) $\qquad \dfrac{dX_1}{dt} = k^+(X_1(t))C(0,t) - k^-(X_1(t), X_1(t-\tau))X_1(t),$

(2.1e) $\qquad \dfrac{dX_2}{dt} = k^+(X_2(t))C(L,t) - k^-(X_2(t), X_2(t-\tau))X_2(t).$

Following Das et al. [8], the association rate k^+ is regulated by positive feedback with saturation in the form of an exponential:

(2.2) $\qquad k^+(X) = (k_0^+ + k_n^+(X/C_{\text{sat}})^n)\exp(-X/C_{\text{sat}}), \quad n \geq 2.$

Similarly, the dissociation rate k_- is controlled by negative delayed feedback according to

(2.3) $\qquad k^-(X(t), X(t-\tau)) = k_0^- \left[1 - \dfrac{\epsilon}{2} + \epsilon \dfrac{X(t-\tau)^h}{X(t)^h + X(t-\tau)^h} \right],$

where τ is the time delay, k_0^- is the baseline dissociation rate in the absence of the delayed negative feedback, ϵ represents the strength of the delayed negative feedback, and h is the Hill coefficient. (For a detailed justification of delayed negative feedback as a mechanism for biochemical oscillations, see [14].) Equations (2.1a)–(2.1e) are supplemented by the conservation equation

(2.4) $\qquad \displaystyle\int_0^L C(x,t)dx + X_1(t) + X_2(t) = C_{\text{tot}},$

where C_{tot} is the total number of Cdc42 molecules per unit area.

In the above formulation of the model, we have assumed that L and C_{tot} are fixed. This simplification is based on the observation that cell elongation is much slower than any of the processes associated with the Cdc42 dynamics. In section 4.3, we will explicitly incorporate elongation of the cell by taking L and C_{tot} to grow linearly in time along the lines of Das et al. [8]. In particular, we will determine how diffusion affects the transition from oscillating monopolar (asymmetric) to oscillating bipolar (symmetric) states during cell elongation. We fix the units of concentration

by setting $C_{\text{sat}} = 1$. The unit of time is taken to be minutes (the typical time-scale of binding/unbinding and the delay τ) and the unit of length is taken to be $5\mu m$ (comparable to the initial length of a fission yeast cell immediately following cell division). It follows that after nondimensionalization a diffusion coefficient of $D = 1$ corresponds to $D \approx 0.5\mu m^2/s$ in physical units. The other parameters of the model are taken to be similar to those of Das et al. [8]. Finally, note that in contrast to the PDE-ODE models of Gou et al., we neglect any degradation of Cdc42; this is reasonable over the time-scales of NETO [10, 11]. Moreover, our main interest is how diffusion affects Cdc42 oscillations that exist in the absence of diffusion, rather than exploring diffusion-induced oscillations; the latter appear to require nonzero degradation rates [10, 11].

3. Analysis of the model in the fast diffusion limit. In this section, we show how to recover the DDE model of Das et al. [8] from our PDE-DDE model by taking the diffusion coefficient $D \to \infty$, and then we carry out a detailed analysis of the resulting DDE. This provides the baseline behavior which will be compared with the behavior of the full model for finite D in section 4. If we introduce the small parameter $\epsilon = L^2 k_0^-/D$ for large D, then the leading order terms of the diffusion equation (2.1a) and the boundary conditions give $C(x,t) = C_0(t)$. Using the conservation equation (2.4), we can rewrite $C_0(t)$ as

$$(3.1) \qquad C_0(t) = \frac{C_{\text{tot}} - X_1(t) - X_2(t)}{L}.$$

The DDE model by Das et al. can then be recovered by substituting (3.1) into the DDE of $X_i(t)$. That is,

$$(3.2a) \qquad \frac{dX_1}{dt} = \frac{k^+(X_1)}{L}(C_{\text{tot}} - X_1(t) - X_2(t)) - k^-(X_1(t), X_1(t-\tau))X_1(t),$$

$$(3.2b) \qquad \frac{dX_2}{dt} = \frac{k^+(X_2)}{L}(C_{\text{tot}} - X_1(t) - X_2(t)) - k^-(X_2(t), X_2(t-\tau))X_2(t),$$

For simplicity, we take $k_0^- = 1$ and $C_{\text{sat}} = 1$ in (2.2) and (2.3).

In the absence of a time delay, $\tau = 0$, we numerically determine the steady state solution of the DDE (3.2) as a function of the total Cdc42 concentration C_{tot}; see Figure 3. For small values of C_{tot}, there exists only a stable symmetric steady state. At $C_{\text{tot}} \approx 1.8$, the symmetric steady state solution loses its stability via a supercritical pitchfork bifurcation, resulting in the formation of a pair of stable asymmetric steady states. However, for $C_{\text{tot}} \approx 6.1$ the symmetric state regains stability due to a subcritical pitchfork bifurcation. This leads to a range of values of C_{tot} over which a pair of stable asymmetric steady states coexists with a stable symmetric steady state. As C_{tot} is further increased, the asymmetric steady states disappear via saddle node bifurcations so that one returns to a single stable symmetric state. Following Das et al. [8], suppose that we vary the cell length L and take the total substrate concentration C_{tot} to be a linearly increasing function of cell length L. (The only explicit dependence of cell length in the DDE model (3.2) is that it scales the rates k_0^+ and k_n^+.) In Figure 4(a) we plot the resulting bifurcation diagram in the (X_1, L)-plane. Without time delay, the asymmetric steady state is linearly stable for $L \in (0.25, 1.285)$, while the symmetric steady state is linearly stable for $L > 1.014$. Moreover, at $L_{sd} \approx 1.285$, the asymmetric steady state vanishes through a saddle node bifurcation. Only the symmetric steady state exists and it is linearly stable for $L > L_{sd}$. This suggests that the cell can undergo a transition from monopolar (asymmetric) growth to bipolar (symmetric) growth as the cell length increases (see section 3.2). The critical value of
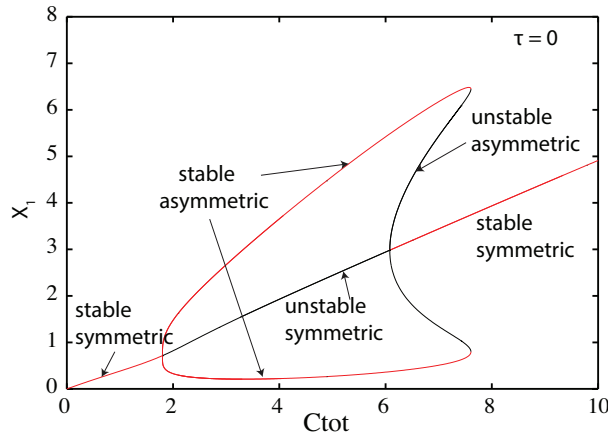
FIG. 3. *Steady state solution of X_1 versus the parameter C_{tot} (in units of C_{sat}) for unit cell length and zero time delay ($\tau = 0$). The bifurcation diagram suggests that there is always a symmetric steady state solution and a pair of asymmetric steady state solutions for the parameter C_{tot} in a certain range. As C_{tot} increases, the symmetric steady state solution loses its stability and the asymmetric steady state solution becomes stable. For large value of C_{tot}, the asymmetric steady state does not exist and the symmetric steady sate is stable. There is also a parameter regime for which stable symmetric and asymmetric steady states coexist. Parameters: $L = 1$, $k_0^+ = 2.25$, $k_n^+ = 6.467$, $n = 4$, $k_0^- = 1$, $\epsilon = 0.5375$, $h = 40$.*
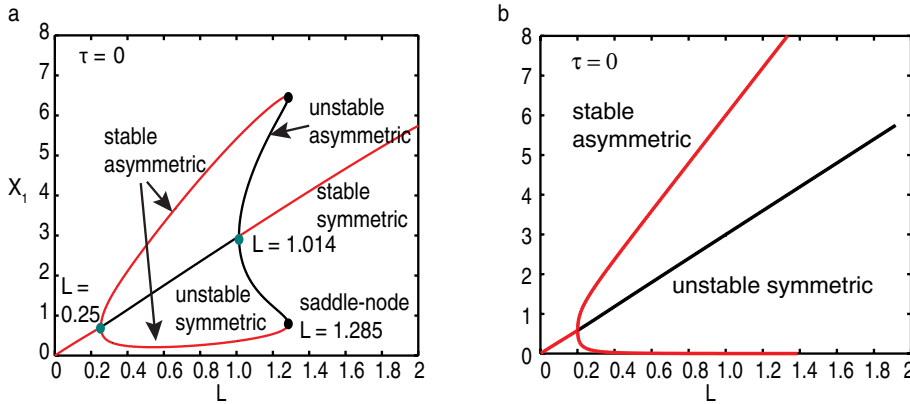

FIG. 4. *Bifurcation diagrams in the (L, X_1) plane for the DDE model (3.2) with $C_{\text{tot}}/L = 6$ and zero delays. (a) Full model. The stable symmetric and asymmetric steady states coexist for a small range of $L \in [1.014, 1.285]$. For $L > 1.285$, the asymmetric steady state vanishes through a saddle-node bifurcation. (b) Nonsaturating positive feedback $k^+(x) = k_0^+ + k_n^+ x^n$. The saddle node point where the stable asymmetric state vanishes is no longer observed. Other parameters are the same as Figure 3.*

L at the saddle node point is dependent on $C_{\text{tot}} = C_0$ at $L = L_0 = 1$ and the strength of the positive feedback $k^+(x)$. If we assume there is no saturation in the positive feedback by dropping the exponential term in (2.2), that is,

$$k^+(X) = (k_0^+ + k_n^+(X/C_{\text{sat}})^n), \quad n \geq 2,$$

then the saddle node point is not observed and the symmetric steady state cannot be stabilized as L increases; see Figure 4(b).
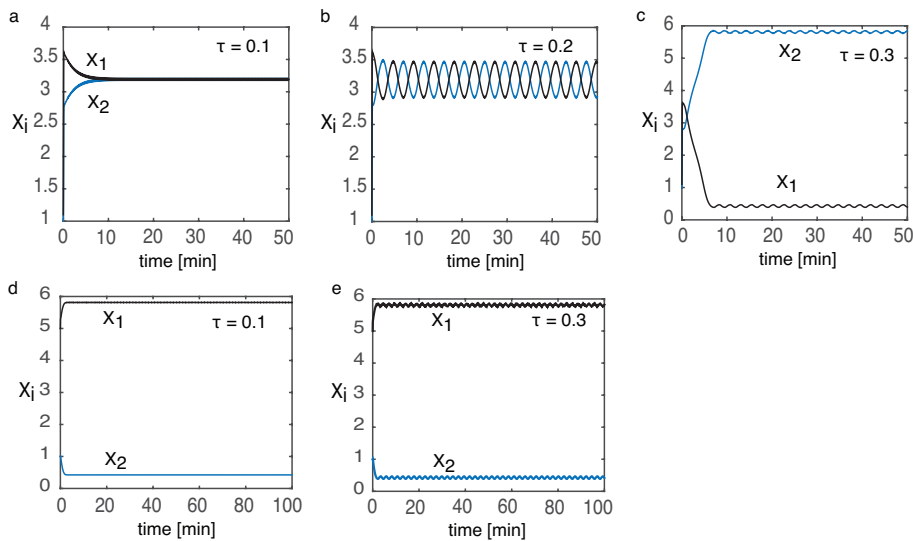
FIG. 5. *Numerical solutions of the DDE model for different time delays and initial conditions.* (a)–(c) *Initial condition* $X_1(t) = 1.1$, $X_2(t) = 1$, $-\tau \leq t \leq 0$. (d)–(e) *Initial condition* $X_1(t) = 5$, $X_2(t) = 1.1$, $-\tau \leq t \leq 0$. *Here* $C_{\text{tot}} = 6.5$, $L = 1$, *and other parameters are the same as Figure* 3.

3.1. Delay-induced oscillations (fixed length). Next, we explore the effects of a nonzero time delay for a fixed value of C_{tot}. As expected, we find that delayed negative feedback can give rise to oscillations. In Figure 5, we plot the numerical solution of the DDE (3.2) for different choices of the time delay τ. For the sake of illustration, we choose $C_{\text{tot}} = 6.5$ so that the symmetric and asymmetric states coexist when $\tau = 0$; see Figure 3. In Figures 5(a)–(c) the initial condition is taken to be close to the symmetric steady state solution with $X_1(t) = 1$, $X_2(t) = 1$ for all $-\tau \leq t \leq 0$. For small time delays, the symmetric steady state solution remains stable. However, as τ is increased the steady state destabilizes, and a periodic, symmetric antiphase solution emerges. When the delay is further increased, the system switches to an asymmetric antiphase solution. One possible reason is that the basin of the attraction of the symmetric steady state is small for small τ. In Figures 5(d), (e), we plot the corresponding numerical solution when the initial condition is taken to be near the asymmetric steady state solution. For a range of values C_{tot}, the stable asymmetric branch can also go unstable to oscillations if the delay τ crosses a threshold from below; see; Figure 6(a).

In order to determine the critical time delay at a Hopf bifurcation point, we perform a linear stability analysis of the DDE model for a fixed length $L = L_0$: Setting

$$F(X_1, X_2) = \frac{1}{L_0} k^+(X_1)(C_{\text{tot}} - X_1(t) - X_2(t)) - k^-(X_1(t), X_1(t-\tau))X_1(t),$$

with $L_0 = 1$, the linearized system near the steady state $(\overline{X}_1, \overline{X}_2)$ is

$$(3.3) \qquad \frac{d}{dt} \begin{pmatrix} y_1(t) \\ y_2(t) \end{pmatrix} = \begin{pmatrix} F_{11} & F_{12} \\ F_{21} & F_{22} \end{pmatrix} \begin{pmatrix} y_1(t) \\ y_2(t) \end{pmatrix} - \frac{\epsilon h}{4} \begin{pmatrix} y_1(t-\tau) \\ y_2(t-\tau) \end{pmatrix},$$
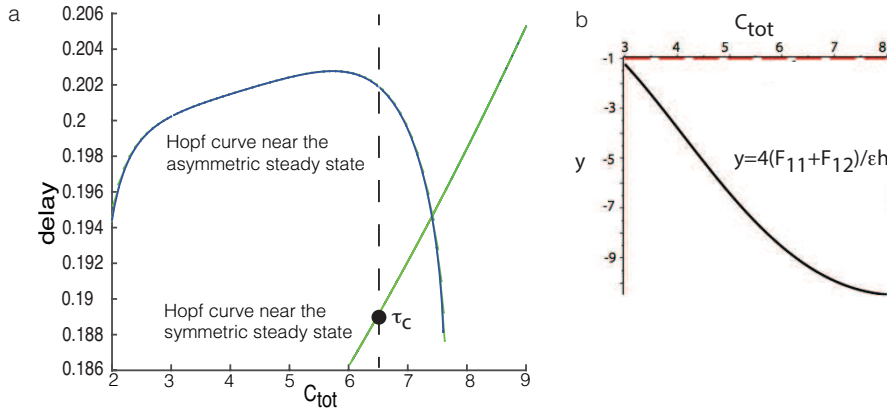
FIG. 6. (a) *Hopf bifurcation curves for the symmetric steady state (green) and the asymmetric steady state (blue) as a function of C_{tot} for fixed cell length $L_0 = 1$. The dashed line indicates the value of C_{tot} used in Figure 4 and the critical delay τ_c for oscillations is shown. Other parameters are the same as Figure 3. (b) Numerical check that $4(F_{11} + F_{12})/h\epsilon < -1$ for the given choice of parameters. Hence, the necessary condition (3.5) for the existence of an in-phase solution cannot hold.*

where

$$F_{11} = \frac{\partial F}{\partial X_1}(\overline{X}_1, \overline{X}_2) = \frac{nk_n^+ \overline{X}_1^{n-1}}{L_0}(C_{\text{tot}} - \overline{X}_1 - \overline{X}_2)e^{-\overline{X}_1}$$
$$- \frac{k_0^+ + k_n^+ \overline{X}_1^n}{L_0}(C_{\text{tot}} - \overline{X}_1 - \overline{X}_2 + 1)e^{-\overline{X}_1} - \left(1 - \frac{\epsilon h}{4}\right),$$

$$F_{12} = \frac{\partial F}{\partial X_2}(\overline{X}_1, \overline{X}_2) = -\frac{k_0^+ + k_n^+ \overline{X}_1^n}{L_0}e^{-\overline{X}_1},$$

and

$$F_{21} = \frac{\partial F}{\partial X_1}(\overline{X}_2, \overline{X}_1), \quad F_{22} = \frac{\partial F}{\partial X_2}(\overline{X}_2, \overline{X}_1).$$

Consider the perturbation

$$X_1 = \overline{X}_1 + \sigma_1 e^{\lambda t}, \quad X_2 = \overline{X}_2 + \sigma_2 e^{\lambda t}.$$

Substituting it into the linearized DDE gives

$$\lambda \begin{pmatrix} \sigma_1 \\ \sigma_2 \end{pmatrix} = \begin{pmatrix} F_{11} - h\epsilon e^{-\lambda\tau}/4 & F_{12} \\ F_{21} & F_{22} - h\epsilon e^{-\lambda\tau}/4 \end{pmatrix} \begin{pmatrix} \sigma_1 \\ \sigma_2 \end{pmatrix}.$$

For a symmetric steady state we have $F_{11} = F_{22}$ and $F_{12} = F_{21}$, so that the matrix is cyclic and symmetric with the eigenvectors $\sigma_1 = -\sigma_2$ (antiphase) and $\sigma_1 = \sigma_2$ (in-phase). The corresponding eigenvalue equations are

(3.4) $$\left(\lambda - F_{11} + \frac{\epsilon h}{4}e^{-\lambda\tau}\right) + F_{12} = 0, \quad \left(\lambda - F_{11} + \frac{\epsilon h}{4}e^{-\lambda\tau}\right) - F_{12} = 0.$$

In order to identify a Hopf bifurcation point, we set $\lambda = i\omega$ in (3.4) and equate real and imaginary parts. This yields the pair of equations

(3.5) $$\omega - \frac{\epsilon h}{4}\sin(\omega\tau) = 0, \quad \cos(\omega\tau) = \frac{4}{\epsilon h}(F_{11} \pm F_{12}),$$

corresponding to the eigenvectors $\sigma_1 = \pm\sigma_2$. The existence of the solution (ω, τ) requires that

$$(3.6) \qquad \left| \frac{4}{\epsilon h}(F_{11} \pm F_{12}) \right| \leq 1.$$

In the asymmetric case we have the characteristic equation

$$(3.7) \qquad \left(\lambda - F_{11} + \frac{\epsilon h}{4}e^{-\lambda\tau} \right) \left(\lambda - F_{22} + \frac{\epsilon h}{4}e^{-\lambda\tau} \right) - F_{12}F_{21} = 0.$$

Again we set $\lambda = i\omega$ in (3.7) and equate real and imaginary parts:

$$(3.8a) \qquad \left[\frac{\epsilon h}{4}\cos(\omega\tau) - F_{11} \right] \left[\frac{\epsilon h}{4}\cos(\omega\tau) - F_{22} \right] - \left(\omega - \frac{\epsilon h}{4}\sin(\omega\tau) \right)^2 - F_{12}F_{21} = 0,$$

$$(3.8b) \qquad \left[\omega - \frac{\epsilon h}{4}\sin(\omega\tau) \right] \left[\frac{\epsilon h}{2}\cos(\omega\tau) - F_{11} - F_{22} \right] = 0.$$

Noting that $F_{12} < 0$ and $F_{21} < 0$, we have

$$\left[\frac{\epsilon h}{4}\cos(\omega\tau) - F_{11} \right] \left[\frac{\epsilon h}{4}\cos(\omega\tau) - F_{22} \right] = \left(\omega - \frac{\epsilon h}{4}\sin(\omega\tau) \right)^2 + F_{12}F_{21} > 0.$$

It follows that

$$\frac{\epsilon h}{2}\cos(\omega\tau) - F_{11} - F_{22} \neq 0,$$

and (3.8) can be simplified as

$$(3.9a) \qquad \omega - \frac{\epsilon h}{4}\sin(\omega\tau) = 0,$$

$$(3.9b) \qquad \left[\frac{\epsilon h}{4}\cos(\omega\tau) - F_{11} \right] \left[\frac{\epsilon h}{4}\cos(\omega\tau) - F_{22} \right] = F_{12}F_{21}.$$

We now solve the two different systems (3.5) and (3.9) numerically. In Figure 6, we plot the Hopf bifurcation curves in the (C_{tot}, τ)-plane for the stable symmetric and asymmetric steady states. Note that for the parameter set chosen in Figure 3, there is no solution (ω, τ) of (3.9) such that the eigenvector $\sigma_1 = \sigma_2$. In Figure 6(b), we check the necessary condition (3.6) for the existence of in-phase solution for the symmetric steady state. The result shows that $4(F_{11} + F_{12})/h\epsilon < -1$ and hence the condition (3.6) for the existence of in-phase solution is not satisfied. It follows that oscillations bifurcating from the symmetric and asymmetric steady states are antiphase. (We find, however, that in-phase oscillations can exist if the strength of the negative feedback ϵ is sufficiently strong or the nonlinearity h is sufficiently high.) In Figure 7, we take $C_{tot} = 6.5$ and plot the amplitude and period of the periodic solutions branching from the symmetric and asymmetric steady states as a function of time delay. For the periodic solution branching from the symmetric steady state, the period increases dramatically at $\tau \approx 0.26$. This suggests that there is a homoclinic orbit resulting from the collision of the symmetric limit cycle with the unstable asymmetric fixed point; see Figure 3. In Figure 8, we plot the numerical solution as a function of time with time delay $\tau = 0.263$ and $\tau = 0.2632$. We find that as the time delay crosses $\tau = 0.263$, the numerical solution evolves to the periodic solution branching from the asymmetric steady state; see Figure 8(b).
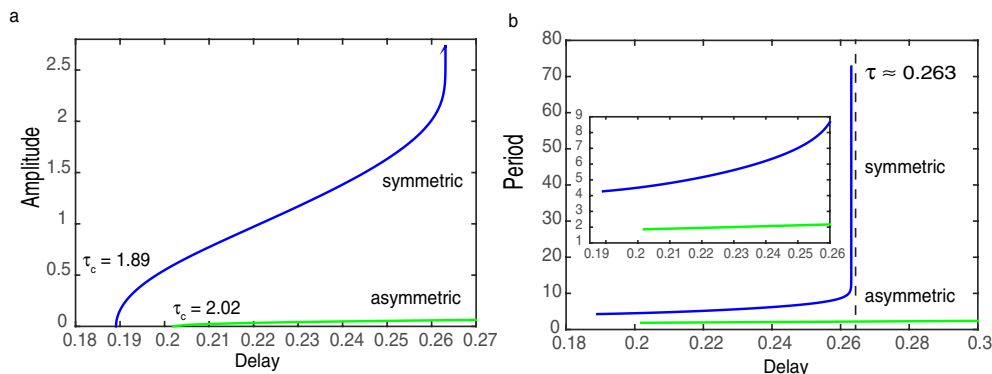
FIG. 7. *Amplitude and period of the periodic solution as a function of the time delay with* $C_{\mathrm{tot}} = 6.5$ *and* $L_0 = 1$. *Blue: result of the periodic solution branching from the symmetric steady state. Green: result of the periodic solution branching from the asymmetric steady state. At time delay* $\tau \approx 0.263$, *the period of the periodic solution branching from the symmetric steady state increases dramatically. It suggests that there is possibly a homoclinic or heteroclinic bifurcation. Other parameters are the same as in Figure* 3.
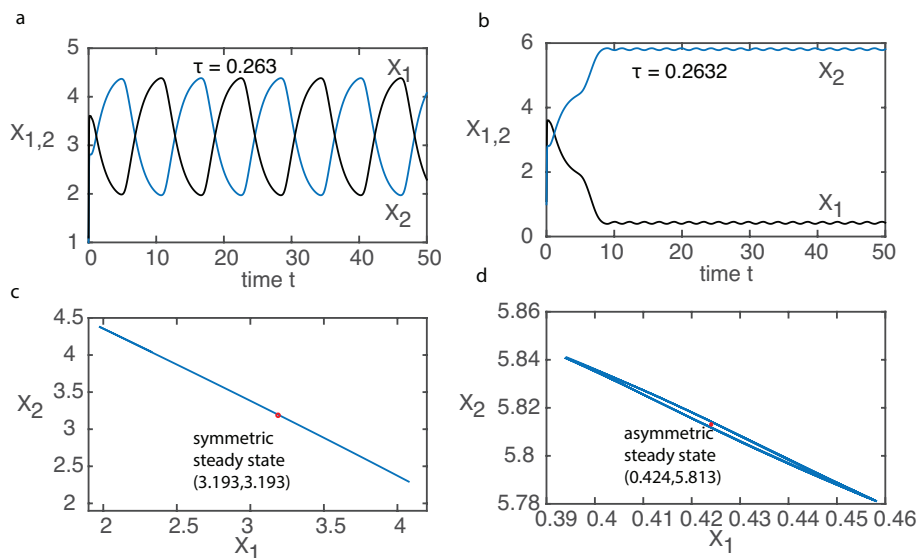

FIG. 8. *Switch from a periodic solution branching from the symmetric steady state to a periodic solution near the asymmetric steady state at time delay* $\tau \approx 0.263$. (a), (b) $X_{1,2}$ *vs* t. (c), (d) *periodic solution in* (X_1, X_2) *plane. Other parameters are the same as in Figure* 3.

3.2. Delay-induced oscillations (varying length). It is straightforward to use the simplified DDE model of Das et al. [8] to investigate the effects of cell elongation. For the sake of illustration, suppose that both L and C_{tot} increase linearly with time at a rate γ. That is, we modify (3.2) by taking

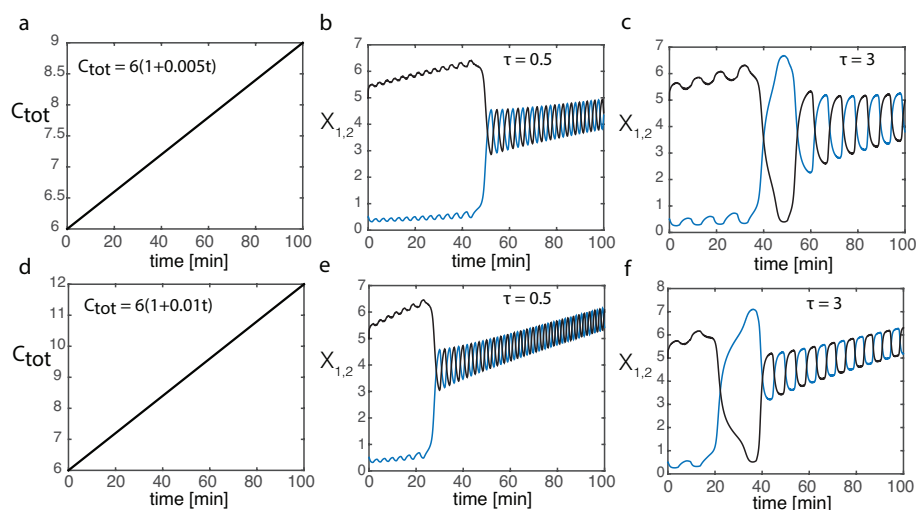$$(3.10) \qquad L(t) = L_0[1 + \gamma t], \quad C_{\mathrm{tot}}(t) = C_0[1 + \gamma t],$$

FIG. 9. *Numerical solutions of the DDE model with* $C_{\text{tot}}(t) = 6(1 + \gamma t)$ *and* $L(t) = 1 + \gamma t$. (a) C_{tot} *versus time t for* $\gamma = 0.005$. (b), (c) *Numerical solutions of* $X_{1,2}(t)$ *for* $\gamma = 0.005$ *and* $\tau = 0.5, 3$, *respectively.* (d)–(f) *Corresponding figures for* $\gamma = 0.01$.

where L_0, C_0 are the initial length and total Cdc42 concentration, respectively. It is important to emphasize, however, that in the case of growing cells one can no longer treat the DDE model as the fast diffusion limit of the full PDE-DDE model (2.1a). Indeed, integrating the diffusion equation (2.1a) over the growing interval $[0, L(t)]$ and imposing the boundary conditions gives

$$\int_0^{L(t)} \partial_t C(x,t)dx = -\frac{dX_1}{dt} - \frac{dX_2}{dt}.$$

Differentiating the conservation condition

$$C_{\text{tot}}(t) = \int_0^{L(t)} C(x,t)dx + X_1(t) + X_2(t)$$

then implies that

$$\frac{dC_{\text{tot}}(t)}{dt} = C(L(t),t)\frac{dL}{dt}.$$

This last equation holds in the large D limit for which $C(L(t),t) \to C_0(t)$. However, it is not satisfied by the growth law of (3.10) for which $C_0(t)/L(t) = C_0/L_0$. Such a law is consistent if one takes proper account of diffusion in a linearly growing domain, which involves adding a convection term to the diffusion model (see section 4.3).

Consistent with the numerical results of Das et al. [8], we find that for moderate delays (e.g., $\tau = 0.5$) the numerical solution changes from an asymmetric to a symmetric oscillation; see Figure 9. Moreover, the switch to the symmetric state occurs at a smaller value of L and C_{tot} (smaller times t) for larger τ. Moreover, for larger delays the oscillations become less sinusoidal, the frequency of oscillations decreases, and we observe an additional transition from large amplitude to low amplitude symmetric
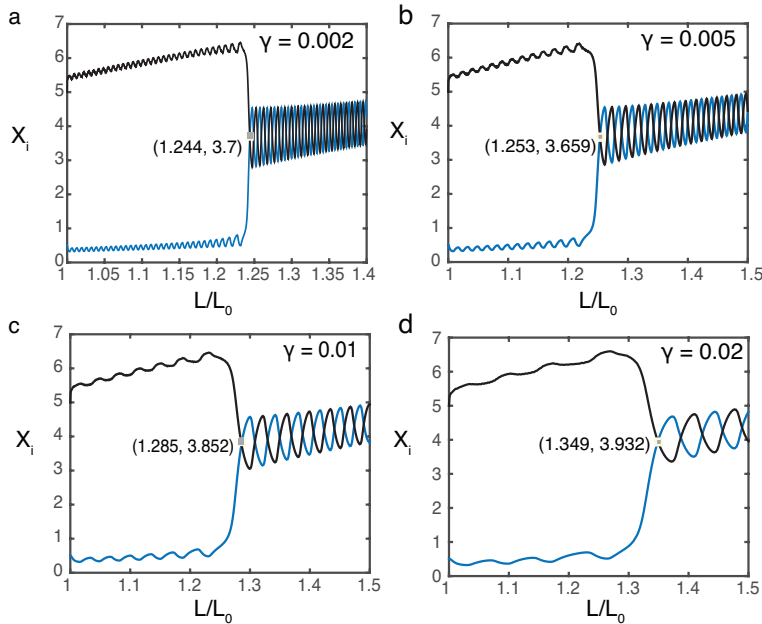
FIG. 10. *Effect of the growth rate on the timing of the switch from asymmetric to symmetric oscillations for the DDE model. As γ is increased, the switch from asymmetric to symmetric oscillation occurs at longer cell lengths. Here $\tau = 0.5$ and other parameters are the same as in Figure* 3.

oscillations; see Figure 9(c), (f). Finally, as shown in Figure 10, the transition between asymmetric and symmetric oscillations occurs at larger cell lengths when the growth rate γ is increased. In conclusion, as previously shown by Das et al. [8], the DDE model reproduces the switch from asymmetric to symmetric Cdc42 oscillations observed experimentally during NETO.

In Figure 11, we plot the Hopf bifurcation curves in the (L, τ)-plane for the stable symmetric and asymmetric steady states. The corresponding Hopf frequency of the Hopf curve branching from the asymmetric fixed point is plotted as a function of the cell length L, or equivalently the critical time delay τ_c in Figure 12. It can be seen that the frequency vanishes at the Hopf bifurcation point, indicative of a Bogdanov–Takens bifurcation. The termination of the asymmetric Hopf branch at a critical cell length L_c is the basic mechanism underlying the switch from an asymmetric oscillation to a symmetric oscillation. It is also consistent with the vanishing of the asymmetric steady states via a saddle node bifurcation when $\tau = 0$; see Figure 4(a). The same basic mechanism holds when bulk diffusion is included using the full PDE-DDE model (2.1a). However, as we will show in section 4, the critical length where the switch occurs is sensitive to the value of the diffusion coefficient.

4. Analysis of the full model. Let us now return to the full PDE-DDE model given by (2.1a)–(2.3), in order to investigate how the switch from asymmetric to symmetric oscillations depends on bulk diffusion. For the moment we take L and C_{tot} to be fixed with C_{tot} treated as a bifurcation parameter. We also perform the rescalings $x \to \widetilde{x} = x/L$, $C \to \widetilde{C} = CL$, and $D \to \widetilde{D} \equiv D/L^2$. The only dependence on L then appears through the association rate k_+, as in the pure DDE model. The
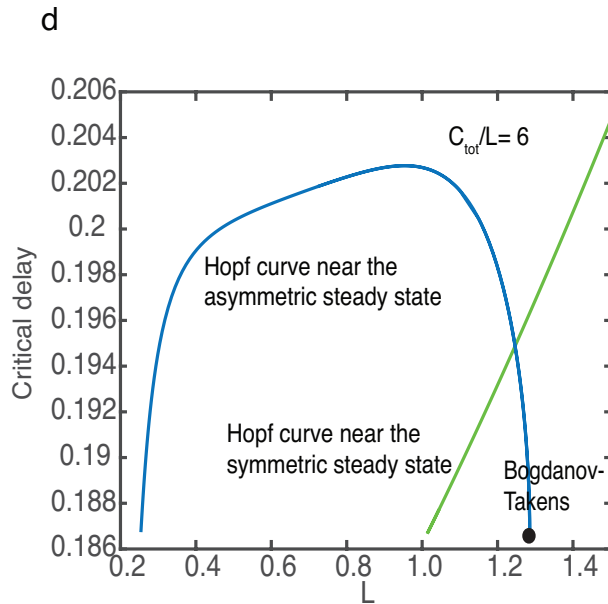
FIG. 11. *Hopf bifurcation curves for the symmetric steady state (green) and the asymmetric steady state (blue) in the (L, τ) plane with $C_{\text{tot}} = 6L$. The Hopf curve for the asymmetric steady state iexists for $L \in (0.25, 1.28)$, while the Hopf curve for the symmetric steady state is plotted for $L > 1.014$. Other parameters are the same as in Figure 3.*
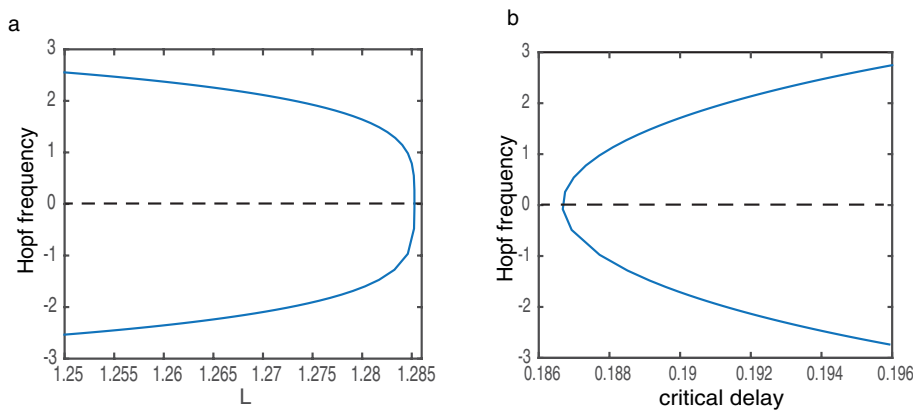

FIG. 12. *Plot of frequency along the Hopf curve branching from the asymmetric steady state as a function of* (a) *cell length L and* (b) *critical delay τ. Near $(\tau, L) \approx (0.18, 1.285)$, the frequency is zero indicative of a Bogdanov–Takens bifurcation. Other parameters are the same as in Figure 3.*

steady state solution for the bulk concentration C satisfies (after dropping the tilde)

$$C''(x) = 0, \quad C'(0) = C'(1) = 0.$$

Hence $C(x)$ is homogeneous, i.e., $C(x) = \overline{C}$. The conservation equation of the total amount of substrate requires that

$$\int_0^1 \overline{C} dx + X_1 + X_2 = C_{\text{tot}}.$$

It follows that $\overline{C} = C_{\text{tot}} - X_1 - X_2$. The steady state solution $(\overline{X}_1, \overline{X}_2)$ satisfies

$$0 = \frac{k^+(\overline{X}_1)}{L}(C_{\text{tot}} - \overline{X}_1 - \overline{X}_2) - k^-(\overline{X}_1, \overline{X}_1)\overline{X}_1,$$

$$0 = \frac{k^+(\overline{X}_2)}{L}(C_{\text{tot}} - \overline{X}_1 - \overline{X}_2) - k_-(\overline{X}_2, \overline{X}_2)\overline{X}_2.$$

Note that the PDE-DDE has the same steady state solution as the DDE model and there exist a symmetric steady state solution $(\overline{X}_1 = \overline{X}_2)$ and an asymmetric steady state solution $(\overline{X}_1 \neq \overline{X}_2)$ for different choices of total substrate concentration C_{tot}; see Figure 2.

4.1. Linear stability analysis. Consider the perturbation near the steady state $(C_0, \overline{X}_1, \overline{X}_2)$,

$$C(x, t) = \overline{C} + e^{\lambda t}\eta(x), \quad X_i(t) = \overline{X}_i + e^{\lambda t}\phi_i.$$

Substituting into the linearized PDE-DDE model near the steady state solution gives

(4.1a) $\qquad D\dfrac{\partial^2 \eta(x)}{\partial x^2} = \lambda \eta(x), \quad 0 < x < 1,$

(4.1b) $\qquad D\partial_x \eta(0) = \dfrac{k^+(\overline{X}_1)}{L}\eta(0) + \left[\dfrac{k'_+(\overline{X}_1)}{L}\overline{C} - \left(1 - \dfrac{\epsilon h}{4} + \dfrac{\epsilon h}{4}e^{-\lambda \tau}\right)\right]\phi_1 = \lambda \phi_1,$

(4.1c) $\qquad -D\partial_x \eta(1) = \dfrac{k^+(\overline{X}_2)}{L}\eta(1) + \left[\dfrac{k'_+(\overline{X}_2)}{L}\overline{C} - \left(1 - \dfrac{\epsilon h}{4} + \dfrac{\epsilon h}{4}e^{-\lambda \tau}\right)\right]\phi_2 = \lambda \phi_2,$

and

(4.2a) $\qquad \left[\lambda + 1 - \dfrac{\epsilon h}{4}(1 - e^{-\lambda \tau}) - \dfrac{k'_+(\overline{X}_1)}{L}\overline{C}\right]\phi_1 = \dfrac{k^+(\overline{X}_1)}{L}\eta(0),$

(4.2b) $\qquad \left[\lambda + 1 - \dfrac{\epsilon h}{4}(1 - e^{-\lambda \tau}) - \dfrac{k'_+(\overline{X}_2)}{L}\overline{C}\right]\phi_2 = \dfrac{k^+(\overline{X}_2)}{L}\eta(1),$

where $k'_+(\overline{X}) = dk^+(X)/dX|_{X=\overline{X}}$. Rewriting (4.2) gives

(4.3) $\qquad \phi_1 = B_1(\lambda, \tau)\eta(0), \quad \phi_2 = B_2(\lambda, \tau)\eta(1),$

with

$$B_i(\lambda, \tau) = \frac{k^+(\overline{X}_i)/L}{\lambda + 1 - \frac{\epsilon h}{4}(1 - e^{-\lambda \tau}) - k'_+(\overline{X}_i)\overline{C}/L}.$$

Substituting (4.3) into the boundary conditions for $\eta(x)$ yields the following nonlinear boundary value problem:

$$D\frac{\partial^2 \eta(x)}{\partial x^2} = \lambda \eta(x), \quad 0 < x < 1, \, t > 0,$$

$$D\partial_x \eta(0) = \lambda B_1(\lambda, \tau)\eta(0),$$

(4.4) $\qquad\qquad -D\partial_x \eta(1) = \lambda B_2(\lambda, \tau)\eta(1).$

The solution $\eta(x)$ can be expressed in the form

$$(4.5) \qquad \eta(x) = \frac{\eta_0 + \eta_1}{2} \frac{\cosh(\sqrt{\lambda/D}(x - \frac{1}{2}))}{\cosh(\frac{1}{2}\sqrt{\lambda/D})} + \frac{\eta_1 - \eta_0}{2} \frac{\sinh(\sqrt{\lambda/D}(x - \frac{1}{2}))}{\sinh(\frac{1}{2}\sqrt{\lambda/D})},$$

where $\eta_0 = \eta(0)$ and $\eta_1 = \eta(1)$. The boundary conditions then require

$$(4.6) \qquad \begin{pmatrix} \mathcal{A}_+(\lambda) + \lambda B_1(\lambda, \tau) & \mathcal{A}_-(\lambda) \\ \mathcal{A}_-(\lambda) & \mathcal{A}_+(\lambda) + \lambda B_2(\lambda, \tau) \end{pmatrix} \begin{pmatrix} \eta_0 \\ \eta_1 \end{pmatrix} = 0,$$

where

$$(4.7) \qquad \mathcal{A}_\pm(\lambda) = \sqrt{\lambda D} \frac{\tanh(\frac{1}{2}\sqrt{\lambda/D}) \pm \coth(\frac{1}{2}\sqrt{\lambda/D})}{2}.$$

Setting the determinant to zero and dividing through by λD gives

$$(4.8) \qquad \frac{\lambda}{D} B_1 B_2 + (B_1 + B_2) \sqrt{\frac{\lambda}{D}} \frac{\tanh(\frac{1}{2}\sqrt{\lambda/D}) + \coth(\frac{1}{2}\sqrt{\lambda/D})}{2} + 1 = 0.$$

The presence of terms involving $\sqrt{\lambda/D}$ means that we have to introduce a branch cut in the complex λ-plane along $(-\infty, 0]$. Fortunately, for finite D, L this does not affect the eigenvalue relation (4.8) since, as $\lambda \to 0$, we have $\tanh(\sqrt{\lambda/4D}) \to \sqrt{\lambda/4D}$ and $\coth(\sqrt{\lambda/4D}) \to \sqrt{4D/\lambda}$, that is, any square roots in (4.8) cancel. However, care has to be taken in the limit $D \to 0$ ($D/(k_0^- L^2) \to 0$ in dimensionless units) since, up to exponentially small errors, $\eta(x) \approx e^{-\sqrt{\lambda/4D}x}$ such that (4.8) reduces to

$$\frac{\lambda}{D} B_1 B_2 + (B_1 + B_2) \sqrt{\frac{\lambda}{D}} + 1 = 0.$$

One can no longer eliminate the square roots and there is a continuous spectrum in addition to a discrete spectrum. We will avoid these complexities here by taking $D > 0$.

Note that (4.3) and (4.8) are well-defined provided that the denominators of the function $B_{1,2}(\lambda, \tau)$ are nonzero. Therefore, we need to check that the boundary value problem still makes sense in the singular limit. Let

$$A(\lambda, \tau, \overline{X}_i) = \lambda + \frac{\epsilon h}{4} e^{-\lambda \tau} + 1 - \frac{\epsilon h}{4} - k'_+(\overline{X}_i) \overline{C}/L,$$

and consider the eigenvalue problem associated with the symmetric steady state solution $\overline{X}_1 = \overline{X}_2 > 0$. If $A(\lambda, \tau, \overline{X}_1) = 0$, then (4.3) requires that

$$\eta(0) = \eta(1) = 0.$$

It is known that the Dirichlet boundary value problem (4.1a) of $\eta(x)$ has only a trivial solution, i.e., $\eta(x) = 0$. To solve for (ϕ_1, ϕ_2), we substitute $\eta(x) = 0$ into the boundary conditions (4.1b) and (4.1c). It follows that

$$0 = \left[1 - \frac{\epsilon h}{4} + \frac{\epsilon h}{4} e^{-\lambda \tau} - \frac{k'_+(\overline{X}_i)}{L} \overline{C} \right] \phi_i = -\lambda \phi_i, \quad i = 1, 2,$$

with the first identity holding since $A(\lambda, \tau, \overline{X}_i) = 0$. Noting that $\lambda = 0$ is not a solution of $A(\lambda, \tau, \overline{X}_i) = 0$, it follows that $\phi_1 = \phi_2 = 0$. Therefore, if $A(\lambda, \tau, \overline{X}_i) = 0$, the

associated solution $(\eta(x), \phi_1, \phi_2)$ is trivial. Hence, we can assume that $A(\lambda, \tau, \overline{X}_i) \neq 0$ for the symmetric steady state, and (4.8) holds. For the symmetric steady state $\overline{X}_1 = \overline{X}_2$, we have $B_1 = B_2$ and the resulting cyclic matrix (4.6) has the eigenvectors $(1,1)^T, (1,-1)^T$. It follows that $\mathcal{A}_+(\lambda) \pm \mathcal{A}_-(\lambda) + \lambda B_1(\lambda, \tau) =$ for the in-phase $(+)$ and antiphase $(-)$ solutions, respectively, with corresponding eigenvalue equations

$$(4.9\text{a}) \qquad B_1 + \sqrt{\frac{D}{\lambda}} \tanh\left(\frac{1}{2}\sqrt{\frac{\lambda}{D}}\right) = 0 \,(\text{in-phase}),$$

$$(4.9\text{b}) \qquad B_1 + \sqrt{\frac{D}{\lambda}} \coth\left(\frac{1}{2}\sqrt{\frac{\lambda}{D}}\right) = 0 \,(\text{antiphase}).$$

Recall that linear stability analysis of the pure DDE model indicated that the oscillation mode is sensitive to the parameters ϵ and h of the negative feedback. With the same parameter set as the DDE model, numerical results of our PDE-DDE model show that the oscillations are also antiphase for different diffusion coefficients (see below). In fact, we can check numerically that the eigenvalue equation (4.9a) does not have a purely imaginary solution $\lambda = i\omega$. To compare with the results of the DDE model, we rewrite (4.9a) as follows:

$$-\frac{1}{B_1} = \sqrt{\frac{\lambda}{D}} \coth\left(\frac{1}{2}\sqrt{\frac{\lambda}{D}}\right) \Rightarrow -\frac{A(\lambda, \tau, \overline{X}_1)}{k^+(\overline{X}_1)/L} = \sqrt{\frac{\lambda}{D}} \coth\left(\frac{1}{2}\sqrt{\frac{\lambda}{D}}\right).$$

Also, noting that

$$F_{12} = -k^+(\overline{X}_1)/L, \quad A(\lambda, \tau, \overline{X}_1) = \lambda + \frac{\epsilon h}{4}\mathrm{e}^{-\lambda\tau} - F_{11} + F_{12},$$

we have

$$(4.10) \qquad \frac{\lambda + \epsilon h \mathrm{e}^{-\lambda\tau}/4 - F_{11} + F_{12}}{F_{12}} = \sqrt{\frac{\lambda}{D}} \cot\left(\frac{1}{2}\sqrt{\frac{\lambda}{D}}\right).$$

Since $\sqrt{\frac{\lambda}{D}} \coth(\frac{1}{2}\sqrt{\frac{\lambda}{D}}) \to 2$ as $D \to \infty$, it follows that (4.10) reduces to

$$\frac{\lambda + \epsilon h \mathrm{e}^{-\lambda\tau}/4 - F_{11} + F_{12}}{F_{12}} = 2 \Rightarrow \lambda + \frac{\epsilon h}{4}\mathrm{e}^{-\lambda\tau} - F_{11} - F_{12} = 0.$$

This is the eigenvalue equation (in-phase) of the DDE model; see (3.4). As shown in Figure 6(b), there is no in-phase solution for the given parameters since $4(F_{11} + F_{12})/h\epsilon < -1$. For a finite D, we can check numerically that there is no solution of $\lambda = i\omega$ by comparing the real parts of (4.10). Defining

$$F_{\mathrm{in}}(\omega) = \sqrt{\frac{i\omega}{D}} \coth\left(\frac{1}{2}\sqrt{\frac{i\omega}{D}}\right), \quad \omega > 0,$$

a numerical plot of the real part of F_{in} indicates that $\mathrm{Re}(F_{\mathrm{in}}) > 2$; see Figure 13. Suppose that there exists a solution (λ, τ) of (4.10) with $\lambda = i\omega$; then the real part of the left-hand side of (4.10) must satisfy

$$\frac{\epsilon h \cos(\omega\tau)/4 - F_{11} + F_{12}}{F_{12}} > 2.$$
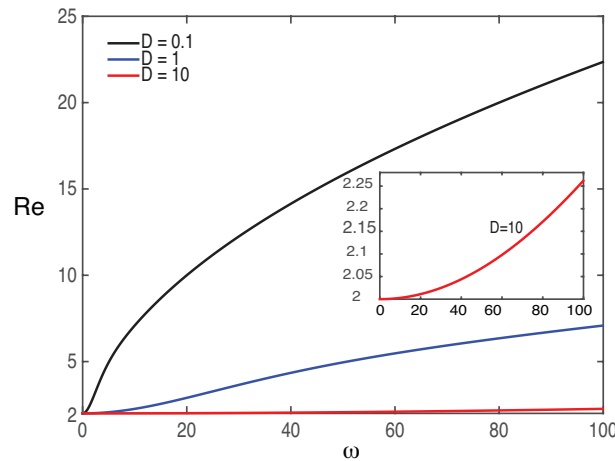
FIG. 13. *Plot of the real part of the function* $F_{\mathrm{in}}(\omega)$ *with different diffusion coefficients.*

Since $F_{12} < 0$, we have

$$\cos(\omega\tau) < 4(F_{11} + F_{12})/\epsilon h < -1.$$

By contradiction, there is no solution of (4.10) with $\lambda = i\omega$. In other words, there is no in-phase oscillation emerging from a Hopf point along the symmetric steady state.

Next, we consider the eigenvalue problem for the asymmetric steady state solution $\overline{X}_1 \neq \overline{X}_2$ where at least B_1 or B_2 is singular. Since $k^+(X)$ is monotonically increasing, it follows that $A(\lambda, \tau, \overline{X}_1)$ and $A(\lambda, \tau, \overline{X}_2)$ cannot attain zero simultaneously. Without loss of generality, we assume that

$$A(\lambda, \tau, \overline{X}_1) = 0, \quad A(\lambda, \tau, \overline{X}_2) \neq 0.$$

It follows that $\eta(0) = 0$ and $\phi_2 = B_2(\lambda, \tau)\eta(1)$. The solution for $\eta(x)$ can be rewritten as

$$\eta(x) = \frac{\eta_1}{2}\left(\frac{\cosh(\sqrt{\lambda/D}(x - \frac{1}{2}))}{\cosh(\frac{1}{2}\sqrt{\lambda/D})} + \frac{\sinh(\sqrt{\lambda/D}(x - \frac{1}{2}))}{\sinh(\frac{1}{2}\sqrt{\lambda/D})}\right).$$

The boundary conditions (4.1b) and (4.1c) require that

$$\phi_1 = \frac{\eta_1}{2}\sqrt{\frac{D}{\lambda}}\left[\coth\left(\frac{1}{2}\sqrt{\lambda/D}\right) - \tanh\left(\frac{1}{2}\sqrt{\lambda/D}\right)\right],$$

$$0 = \left(\sqrt{\lambda D}\frac{\tanh(\frac{1}{2}\sqrt{\lambda/D}) + \coth(\frac{1}{2}\sqrt{\lambda/D})}{2} + \lambda B_2(\lambda, \tau)\right)\eta_1.$$

Hence, in order to have a nontrivial solution, we require

$$A(\lambda, \tau, \overline{X}_1) = 0, \quad \frac{\tanh(\frac{1}{2}\sqrt{\lambda/D}) + \coth(\frac{1}{2}\sqrt{\lambda/D})}{2} + \sqrt{\frac{\lambda}{D}}B_2(\lambda, \tau) = 0.$$

The second equation also arises from taking the limit $B_1 \to \infty$ in (4.8). Note that the root λ of the second equation is dependent on the parameter D, while the root of the first equation is independent of D. For any fixed τ and D, these two equations can be solved numerically.
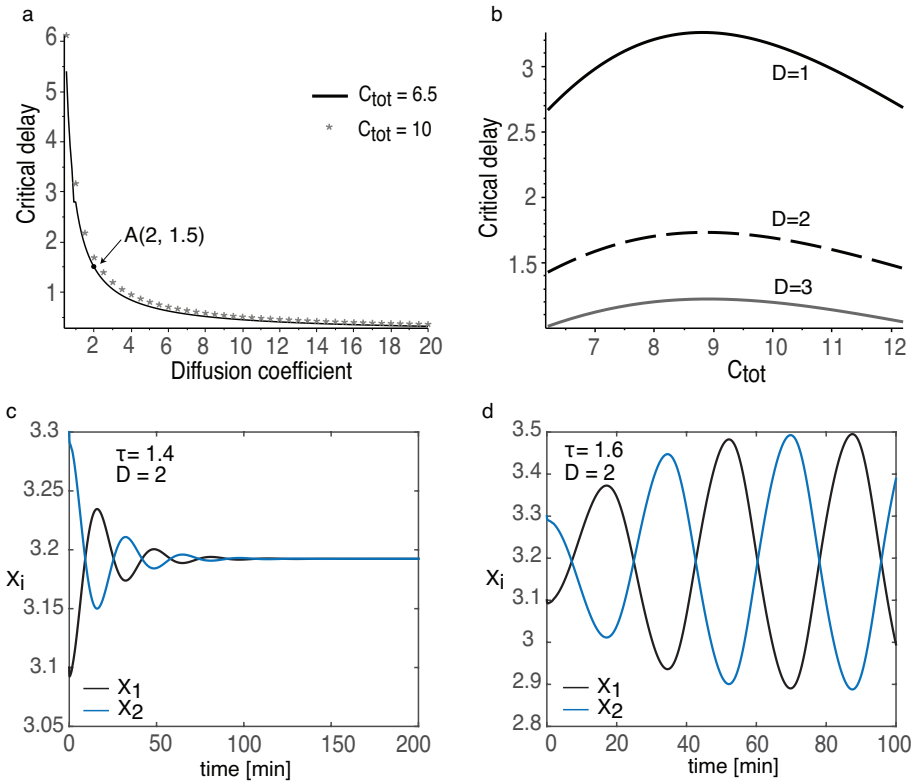
FIG. 14. *Effects of diffusion on Hopf bifurcations from the symmetric steady state.* (a) *Critical delay τ versus diffusion coefficient D. As $D \to \infty$, the critical time delay approaches a horizontal asymptote, which is the same as the DDE model.* (b) *Critical delay τ versus the total substrate concentration C_{tot}.* (c), (d) *Numerical solution of $X_{1,2}$ with (D, τ) below and above the Hopf point A, respectively, indicating that the Hopf bifurcation at A is supercritical and the oscillation mode is antiphase. Baseline parameters: $k_0^+ = 2.25$, $k_n^+ = 6.467$, $n = 4$, $C_{\text{tot}} = 6.5$, $k_0^- = 1$, $\epsilon = 0.5375$, $h = 40$, and $L = 1$. Initial condition: $X_1(t) = 3.1$, $X_2(t) = 3.3$, $C(x, t) = 0.1$ for $-\tau \le t \le 0$.*

4.2. Hopf bifurcations. In the following, we numerically solve the eigenvalue relations for the symmetric and asymmetric steady states in order to determine Hopf bifurcation curves, and we show the results of various numerical simulations. Our main goal is to investigate how bulk diffusion can change the critical time delay for the onset of oscillations.

4.2.1. Case (a). Hopf bifurcation from the symmetric steady state. In Figures 14(a), (b) we plot the critical delay for a Hopf bifurcation from the symmetric steady state as a function of the diffusion coefficient D and total substrate concentration C_{tot}, respectively. Compared to the parameter C_{tot}, the critical time delay is more sensitive to the value of the diffusion coefficient. For small D the critical time delay is relatively large but decreases as D increases. There exists an asymptote of the critical time delay as $D \to \infty$, which agrees with the critical delay for the DDE model by Das et al. [8]; see section 3. For a fixed value of D, the critical time delay has a maximum as the parameter C_{tot} changes from 6 to 12. For an arbitrarily chosen point A $((D, \tau) = (2, 1.5))$ on the Hopf curve in Figure 14(a), we determine the direction of the Hopf bifurcation by solving the PDE-DDE (2.1a) numerically. For a parameter
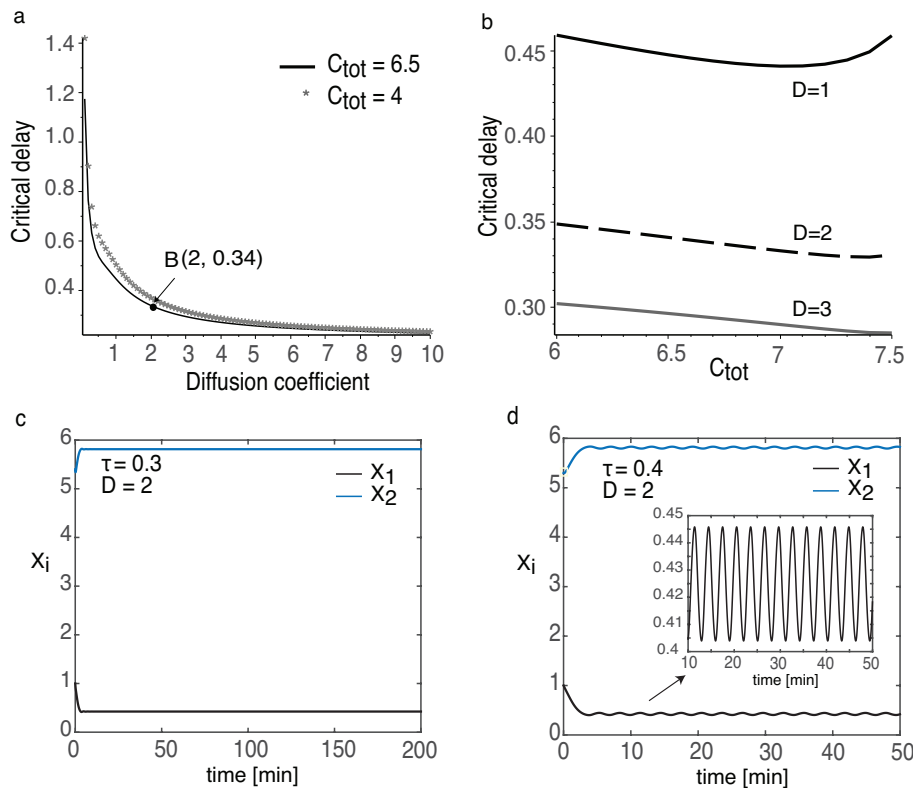
FIG. 15. *Effects of diffusion on Hopf bifurcations from the asymmetric steady state.* (a) *Critical delay τ versus diffusion coefficient D.* (b) *Critical delay τ versus the total substrate concentration C_{tot}.* (c), (d) *Numerical solution of $X_{1,2}$ with (D, τ) below and above the Hopf point B, respectively, indicating that the Hopf bifurcation at B is supercritical. Baseline parameters: $k_0^+ = 2.25$, $k_n^+ = 6.467$, $n = 4$, $C_{\text{tot}} = 6.5$, $k_0^- = 1$, $\epsilon = 0.5375$, $h = 40$. Initial condition: $X_1(t) = 1$, $X_2(t) = 5.3$, $C(x, t) = 0.2$ for $-\tau \leq t \leq 0$.*

set $(D, \tau) = (2, 1.4)$ below the Hopf point, the numerical solution indicates that the steady state solution is stable; see Figure 14(c). For a parameter set $(D, \tau) = (2, 1.6)$ above the Hopf point, the steady state loses its stability and the numerical solution oscillates near the symmetric steady state; see Figure 14(d). This suggests that the Hopf bifurcation at the point A is supercritical.

4.2.2. Case (b). Hopf bifurcation from the asymmetric steady state. For the asymmetric steady state, we plot the Hopf curves and numerical solutions of $X_{1,2}$ in Figure 15. Again the critical time delay decreases as the diffusion coefficient increases, but the critical time delay tends to be smaller than for the symmetric steady state. Recall from the bifurcation diagram of the DDE model (see Figure 3) that there exists a parameter domain $C_{\text{tot}} \in [6.1, 7.6]$ where the symmetric steady state and asymmetric steady state coexist for $\tau = 0$. In Figure 16, we plot the Hopf branches corresponding to the symmetric and asymmetric steady states in this parameter domain for different values of D. Unlike the Hopf curves of the DDE model where the two branches intersect (see Figure 6(a)), no intersection of the Hopf branches is observed for $D = 2$ and $D = 20$. For $D = 2$, the two Hopf curves separate the parameter domain (C_{tot}, τ) into three different regions. In region 1, both of the
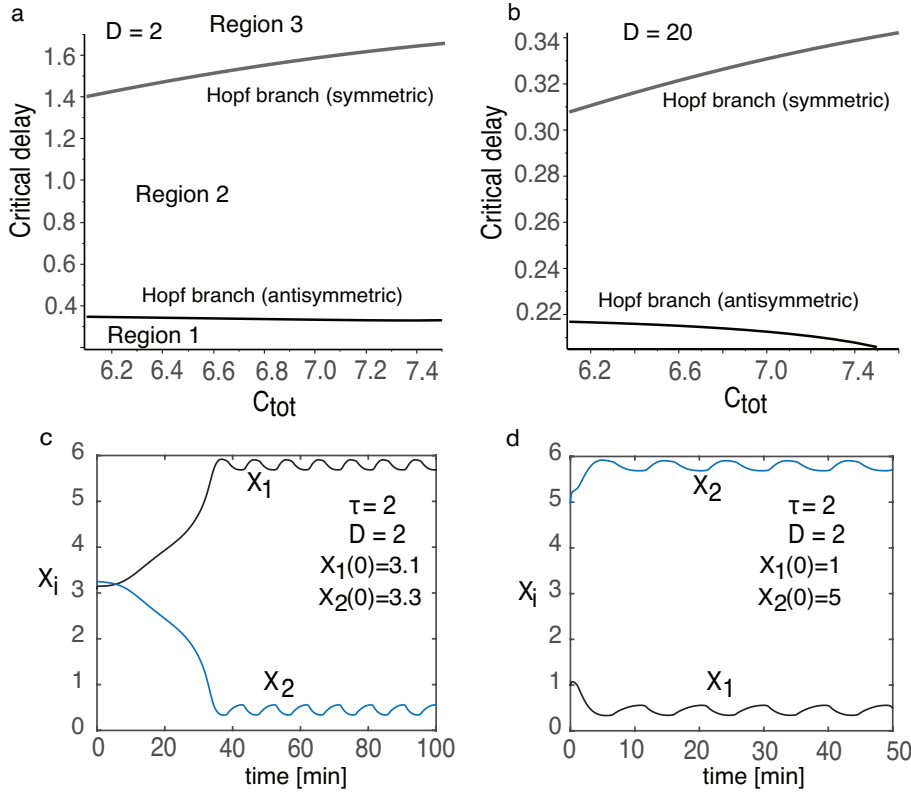
FIG. 16. (a), (b) *Hopf curves along the symmetric and asymmetric steady states as* C_{tot} *changes for* $D = 2, 20$*, respectively.* (c) *Numerical solution of* $X_{1,2}$ *with initial condition:* $C(x, t) = 0.1, X_1(t) = 3.1, X_2(t) = 3.3, -\tau \leq t \leq 0$. (d) *Numerical solution of* $X_{1,2}$ *with initial condition:* $C(x, t) = 0.5, \quad X_1(t) = 1, X_2(t) = 5, \quad -\tau \leq t \leq 0$. *Both of the solutions oscillate near the asymmetric steady state. Baseline parameters:* $D = 2, C_{\text{tot}} = 6.5, L = 1, \tau = 2, k_0^+ = 2.25, k_n^+ = 6.467, n = 4, k_0^- = 1, \epsilon = 0.5375, h = 40$.

steady state solutions are linearly stable. In region 2, the asymmetric steady state is linearly unstable and a small perturbation near the asymmetric steady state generates oscillatory solutions. In region 3, we expect to find both symmetric and asymmetric oscillations. In order to explore this possibility, we plot the numerical solutions for different initial conditions in Figures 16(c), (d). The initial conditions are either near the symmetric steady state,

$$C(x, t) = 0.1, \quad X_1(t) = 3.1, \quad X_2(t) = 3.3, \quad -\tau \leq t \leq 0,$$

or near the asymmetric steady state,

$$C(x, t) = 0.5, \quad X_1(t) = 1, \quad X_2(t) = 5, \quad -\tau \leq t \leq 0.$$

In both cases, oscillations occur around the asymmetric steady state. On the other hand, for smaller time delays in region 3, the first initial condition can lead to symmetric oscillations; see Figure 17. This suggests that the time delay could give rise to spontaneous symmetry breaking.

Figures 16(a), (b) implies that for a finite diffusion coefficient, $D = 2$ and $D = 20$, the critical time delay for the symmetric branch is larger than that for the asymmetric
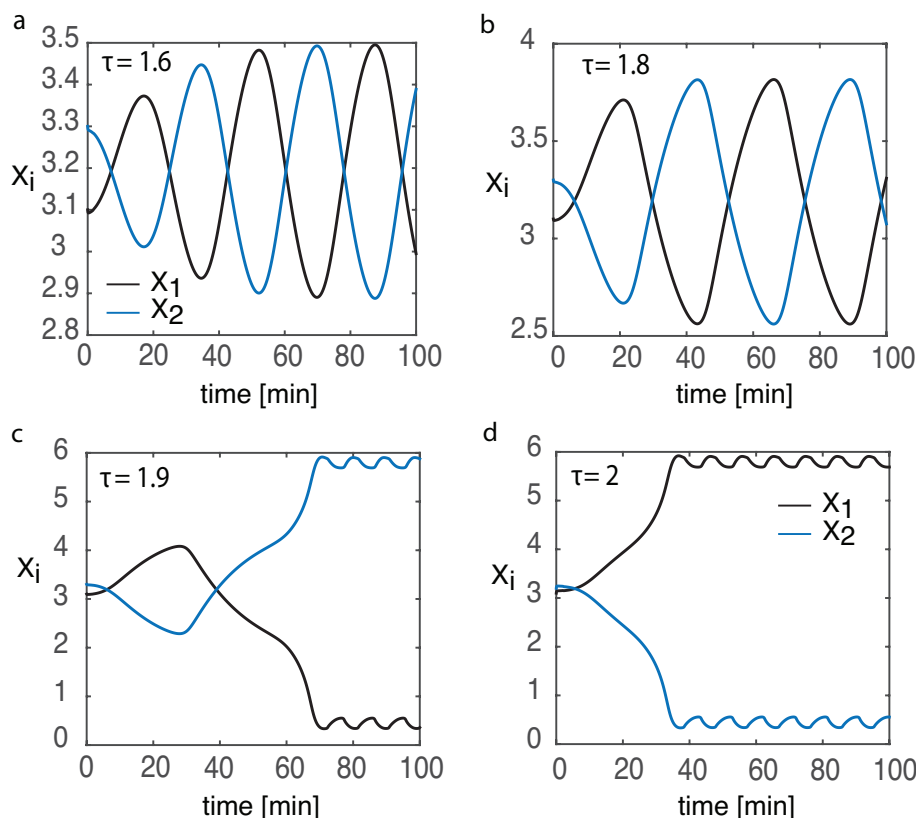
FIG. 17. *Numerical solution with different time delays. As the time delay increases, the amplitude of the oscillation increases. At $\tau = 1.9$, the numerical solution changes from symmetric to asymmetric oscillations. Parameters: $D = 2$, $k_0^+ = 2.25$, $k_n^+ = 6.467$, $n = 4$, $k_0^- = 1$, $\epsilon = 0.5375$, $h = 40$. Initial condition: $X_1(t) = 3.1$, $X_2(t) = 3.3$, $C(x,t) = 0.1$ for $-\tau \leq t \leq 0$.*

branch. This is different from the result of critical time delays for the two branches for the DDE model; see Figure 6(a). To compare the critical time delay in the fast diffusion limit with the DDE model given by (3.2), we plot the Hopf curves in the (D, τ) plane for large D with $C_{\text{tot}} = 6.5, 7.45$, respectively; see Figure 18. For the smaller value $C_{\text{tot}} = 6.5$ and sufficiently large D, the Hopf curve for the symmetric branch decreases faster than that for asymmetric steady state and reaches a smaller asymptote. On the other hand if $C_{\text{tot}} = 7.45$, then the asymptote of the Hopf curve for the symmetric branch is larger than that for the asymmetric branch. The result is consistent with the result of the DDE model; see Figure 6(a).

4.3. NETO. In the DDE model of Cdc42 oscillations by Das et al. [8] and the ODE model of NETO by Cerone, Novák, and Neufeld [5], it is crucial to assume that the total amount of substrate increases as the cell length increases. One possible explanation for this assumption is that a typical cell must double its mass and duplicate its contents so that the new daughter cells can contain the components needed for independent growth and eventual division. Recall that the total amount C_{tot} of Cdc42 per unit area, for fixed length L, is defined by the conservation equation

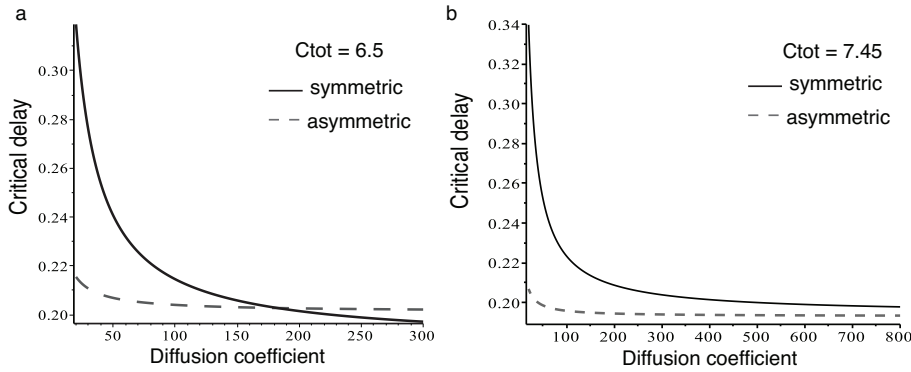$$C_{\text{tot}} = \int_0^L C(x,t)dx + X_1(t) + X_2(t).$$

FIG. 18. *Comparison of effects of diffusion on Hopf bifurcations from the symmetric and asymmetric steady states for a large diffusion coefficient.* (a) $C_{\text{tot}} = 6.5$. (b) $C_{\text{tot}} = 7.45$. *For a wide range of values of diffusion coefficients, the critical time delay at a Hopf bifurcation from the symmetric steady state is larger than that for the asymmetric steady state. This still holds for large D when $C_{\text{tot}} = 7.45$. However, for a smaller value of $C_{tot} = 6.5$ and a sufficiently large $D(> 190)$, the critical time delay at a Hopf bifurcation from the symmetric steady state is smaller than that for the asymmetric steady state. This is consistent with the results for the critical time delay in the DDE model; see Figure* 3. *Baseline parameters:* $k_0^+ = 2.25$, $k_n^+ = 6.467$, $n = 4$, $C_{\text{tot}} = 6.5$, $k_0^- = 1$, $\epsilon = 0.5375$, $h = 40$.

In order to reproduce the experimentally observed switch from asymmetric to symmetric oscillations during NETO, we now modify our PDE-DDE model to take into account diffusion in a growing domain $\Omega_t = [0, L(t)]$, in which the total substrate concentration C_{tot} increase explicitly with respect to time t. We will extend our analysis of diffusion in a growing 1D domain along lines similar to Crampin, Gaffney, and Maini [7], who studied the particular problem of spontaneous pattern formation for a reaction-diffusion equation on a growing domain. We begin by expressing the resulting conservation equation in the form

$$(4.11) \qquad \frac{d}{dt} \int_{\Omega_t} C(x,t)dx + \int_{\Omega_t} \frac{\partial J(x,t)}{\partial x}dx = \frac{dC_{\text{tot}}(t)}{dt}$$

with

$$J(x,t) = -D\frac{\partial C(x,t)}{\partial x}, \quad \int_{\Omega_t} \frac{\partial J(x,t)}{\partial x}dx = \frac{dX_1}{dt} + \frac{dX_2}{dt}.$$

Using the Reynolds transport theorem to evaluate the first term on the left-hand side,

$$(4.12) \qquad \frac{d}{dt} \int_{\Omega_t} C(x,t)dx = \int_{\Omega_t} \left[\frac{\partial C(x,t)}{\partial t} + \frac{\partial [\phi(x,t)C(x,t)]}{\partial x} \right] dx,$$

where $\phi(x,t)$ is the flow of the domain at time t. If we take

$$C_{\text{tot}}(t) = \frac{C_0}{L_0}L(t)$$

with $C_0 = C_{\text{tot}}(0)$, then we obtain the evolution equation

$$(4.13) \quad \frac{\partial C(x,t)}{\partial t} + \frac{\partial [\phi(x,t)C(x,t)]}{\partial x} = D\frac{\partial^2 C(x,t)}{\partial x^2} + \frac{C_0}{L_0}\frac{\dot{\rho}}{\rho}, \quad 0 < x < L(t), \quad t > 0.$$

Let $X \in [0, L_0]$ be the local coordinate system at the initial length L_0. Using a Lagrangian description, we can represent spatial position at time t as

$$x = \Gamma(X, t) = X\rho(t), \quad \rho(0) = 1,$$

with corresponding flow

$$(4.14) \qquad \phi(x, t) = X\dot{\rho} = x\frac{\dot{\rho}}{\rho}.$$

Consistent with the analysis of the DDE model, we take $\rho(t) = 1 + \gamma t$ so that

$$L(t) = L_0(1 + \gamma t).$$

Substitution into (4.13) gives

$$(4.15) \qquad \frac{\partial C(x, t)}{\partial t} + \left(\frac{\dot{\rho}}{\rho}\right)\left(x\frac{\partial C(x, t)}{\partial x} + C(x, t)\right) = D\frac{\partial^2 C(x, t)}{\partial x^2} + \frac{C_0}{L_0}\frac{\dot{\rho}}{\rho}.$$

Following Crampin, Gaffney, and Maini [7], we transform (4.15) to the fixed interval $[0, L_0]$ by performing the change of variables

$$(4.16) \qquad (x, t) \to (\bar{x}, \bar{t}) = \left(\frac{x}{\rho(t)}, t\right).$$

Under this transformation the advection term in (4.15) is eliminated and, on dropping the overbars, we obtain the modified evolution equation

$$(4.17a) \qquad \frac{\partial C(x, t)}{\partial t} = \frac{D}{L(t)^2}\frac{\partial^2 C(x, t)}{\partial x^2} - \left(\frac{\dot{\rho}}{\rho}\right)C(x, t) + \frac{C_0}{L_0}\frac{\dot{\rho}}{\rho}.$$

The boundary conditions are

$$(4.17b) \qquad -\frac{D}{L(t)}\partial_x C(0, t) = -\frac{k^+(X_1(t))}{L(t)}C(0, t) + k^-(X_1(t), X_1(t - \tau))X_1(t),$$

$$(4.17c) \qquad -\frac{D}{L(t)}\partial_x C(L_0, t) = \frac{k^+(X_2(t))}{L(t)}C(L_0, t) - k^-(X_2(t), X_2(t - \tau))X_2(t).$$

The DDE for $X_{1,2}$ are

$$(4.17d) \qquad \frac{dX_1}{dt} = \frac{k^+(X_1(t))}{L(t)}C(0, t) - k^-(X_1(t), X_1(t - \tau))X_1(t),$$

$$(4.17e) \qquad \frac{dX_2}{dt} = \frac{k^+(X_2(t))}{L(t)}C(L, t) - k^-(X_2(t), X_2(t - \tau))X_2(t).$$

In the following we take $L_0 = 1$ and solve the PDE-DDE (4.17a)–(4.17e) numerically on the domain $[0, 1]$.

From our analysis of the pure DDE model in section 3, we expect there to be a switch from an asymmetric oscillation to a symmetric oscillation as the cell grows. However, one major difference between the PDE-DDE model and the DDE model is that in the former case the Hopf curve for symmetric bifurcations lies above the Hopf curve for asymmetric bifurcations, as illustrated in Figure 16 for fixed L. This suggests that when the asymmetric Hopf branch disappears, the symmetric state may

be below its Hopf bifurcation point so that no symmetric oscillations are observed. This is indeed found to be the case, as illustrated in Figure 19 for a small constant growth rate $\gamma = 0.01$. The initial condition is chosen to be near the asymmetric steady state when $C_{\text{tot}} = 6$. For a fixed time delay $\tau = 1.4$ and $D = 2$, the numerical solution of $X_{1,2}$ starts oscillating near the asymmetric steady state and evolves to the symmetric steady state as C_{tot} increases. However, oscillations near the symmetric steady state are not observed, since the time delay is below the critical time delay for $D = 2$. That is, for changing L one can construct Hopf curves similar to those of Figure 16(a) for fixed cell length and show that the system is in region 2. This is different from the behavior of the DDE model shown in Figure 9(b), for which a small time delay (e.g., $\tau = 0.5$) can give rise to both symmetric and asymmetric oscillations. On the other hand, for larger τ and D, the PDE-DDE model does exhibit a transition from an asymmetric to symmetric oscillations as L increases. Moreover, the amplitude of the symmetric oscillations increases as D increases; see Figure 19 (c), (d). In Figure 20, we plot the numerical solution as a function of L/L_0 for different D and growth rates γ. Interestingly, as the growth rate increases from 0.005 to 0.01, we find that the switch from an asymmetric to symmetric oscillations occurs at a relatively larger value of L/L_0, again reflecting a breakdown of the adiabatic approximation. On the other hand, as D is increased, the switch occurs at a smaller value of L/L_0.

5. Discussion. In this paper, we studied a 1D PDE-DDE model for the signaling molecule Cdc42 during cell polarization in fission yeast. The PDE model represents the diffusion of Cdc42 in the cytoplasm, whereas the system of DDEs represents the association and dissociation of Cdc42 at the two end compartments, which are regulated by positive feedback and delayed negative feedback, respectively. In the fast diffusion limit and fixed length, we recovered the DDE model of Das et al. [8]. Using linear stability analysis and numerical simulations, we investigated Hopf bifurcations of the symmetric and asymmetric steady states. We showed that the critical time delay at the Hopf point is sensitive to the diffusion coefficient; as the diffusion coefficient increases, the critical delay decreases and reaches an asymptote. This suggests that the DDE model underestimates the critical time delay. Finally, we solved the diffusion equation on a growing domain under the additional assumption that the total amount C_{tot} of the signaling molecule increases as the cell length increases. We showed that the system undergoes a transition from asymmetric to symmetric oscillations as the cell grows, consistent with experimental findings of "new-end-take-off" in fission yeast. We also found that the critical length where the switch occurs depends on both D and the growth rate.

We note that the particular result concerning the effect of diffusion on the critical time delay for a Hopf bifurcation has previously been shown for a genetic control model by Busenberg and Mahaffy [3, 4]. However, there are several major differences between our model and theirs. First, the genetic control model involves two species, mRNA and a repressor protein, whereas there is only a single chemical component in our model (signaling protein Cdc42). Second, in our model, the delayed negative feedback is incorporated into the boundary conditions, while the delayed feedback in the genetic control model occurs in a reaction term of the repressor protein. Third, the genetic control model consists of two compartments, one of which is well-mixed. Most significantly, our model has both symmetric and asymmetric steady states, while the genetic model has a unique steady state.
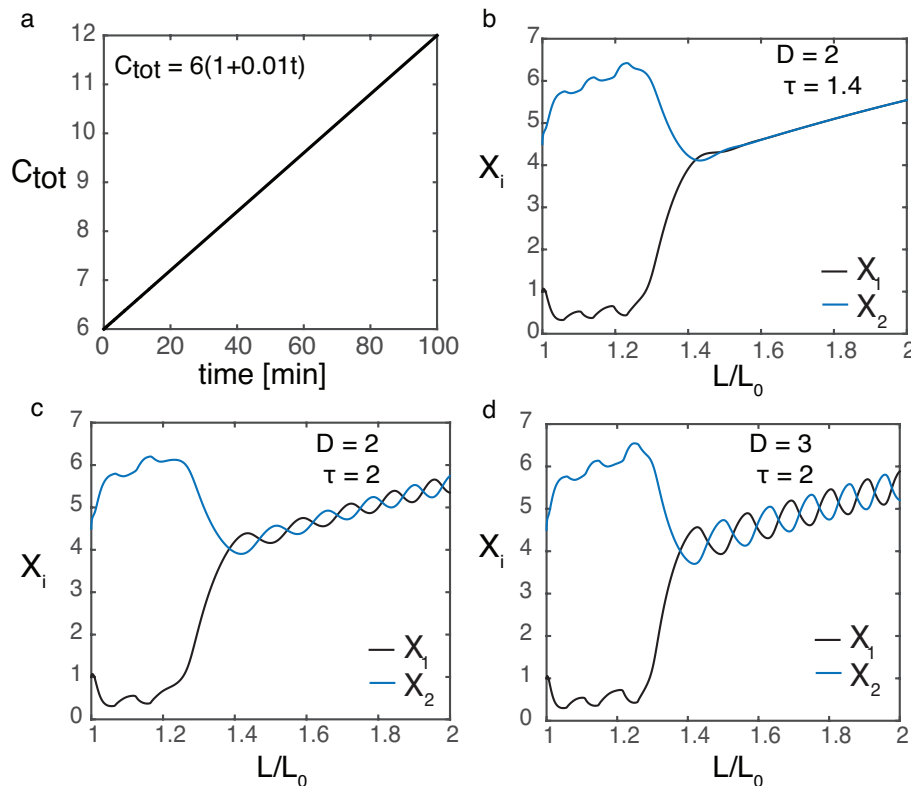
FIG. 19. *Switch from asymmetric to symmetric oscillations with C_{tot} and L slowly increasing functions of time t. For a smaller diffusion coefficient $D = 2$, the time delay $\tau = 1.4$ is not large enough to give rise to symmetric oscillations. On the other hand, for $\tau = 2$ and either $D = 2$ or $D = 3$, the numerical solution changes from asymmetric to symmetric oscillations consistent with the pure DDE model. As the diffusion coefficient increases, the amplitude of the symmetric oscillations also increases. The numerical solution is for the PDE-DDE model (4.17a)–(4.17e). Parameters: $L_0 = 1$, $\gamma = 0.01$, $k_0^+ = 2.25$, $k_n^+ = 6.467$, $n = 4$, $k_0^- = 1$, $\epsilon = 0.5375$, $h = 40$. Initial condition: $X_1(t) = 1$, $X_2(t) = 4.5$, $C(x, t) = 0.5$ for $-\tau \leq t \leq 0$.*

There are a number of possible extensions of our work. First, in this paper we followed Das et al. [8] and took the basic mechanism for generating Cdc42 oscillations to be a negative feedback loop with a discrete delay. Since the precise cause of Cdc42 oscillations is not currently known, it would be worth exploring alternative mechanisms as highlighted by Novak and Tyson [14]. However, we do not expect the basic results of the paper to be altered. Second, our model could be modified to study other signaling molecules that are involved in the polarization of fission yeast such as formin for3p [12]. Third, it would be interesting to consider the full 3D geometry of fission yeast, where bulk diffusion occurs in the cylindrical interior of the cell and the end compartments are treated as hemispherical caps. Finally, from a more general mathematical perspective, our study suggests that it would be worth extending the class of diffusion models considered by Gou et al. [10, 11] to the case where diffusively active compartments evolve according to DDEs.
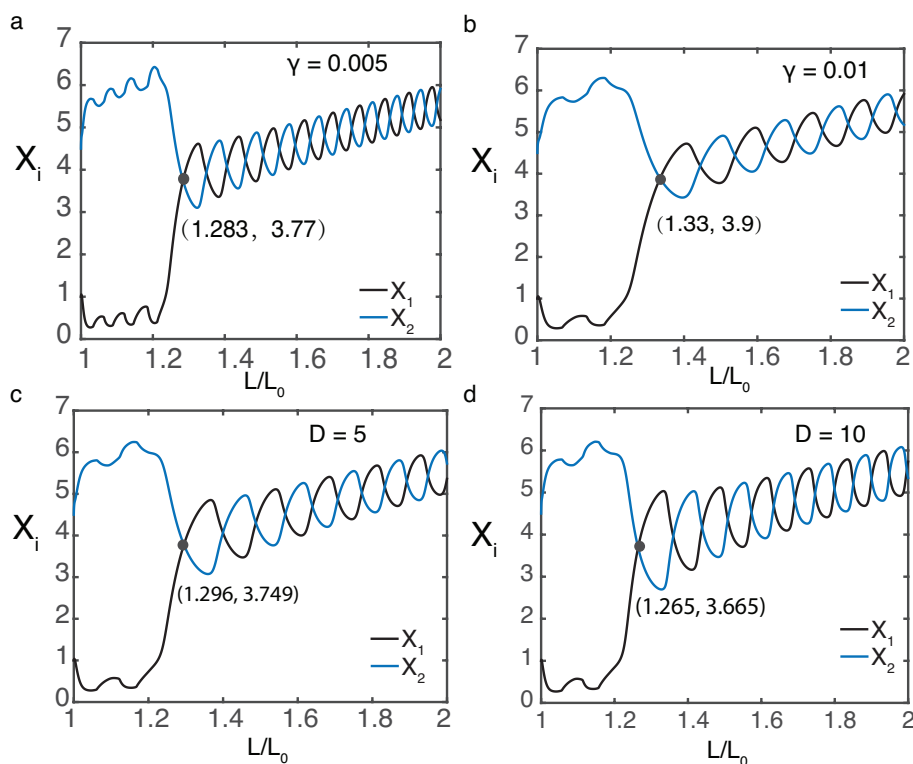
FIG. 20. *Effect of the growth rate and diffusion coefficient on the timing of the switch from asymmetric to symmetric oscillations.* (a), (b) *As γ increased, the switch from asymmetric to symmetric oscillation occurs later.* (c), (b). *On the other hand, as D is increased, the switch occurs earlier. The numerical solution is for the PDE-DDE model* (4.17a)–(4.17e). *Baseline parameters: $D = 3$, $\tau = 3$, $\gamma = 0.01$, $L_0 = 1$. Other parameters are the same as in Figure* 19. *Initial condition: $X_1(t) = 1$, $X_2(t) = 4.5$, $C(x,t) = 0.5$ for $-\tau \leq t \leq 0$.*

REFERENCES

[1] P. C. BRESSLOFF, *Stochastic Processes in Cell Biology,* Springer, New York, 2014.

[2] P. C. BRESSLOFF AND B. XU, *Stochastic active-transport model of cell polarization,* SIAM J. Appl. Math., 75 (2015), pp. 652–678.

[3] S. BUSENBERG AND J. MAHAFFY, *Interaction of spatial diffusion and delays in models of genetic control by repression,* J. Math. Biol., 22 (1985), pp. 313–333.

[4] S. BUSENBERG AND J. MAHAFFY, *The Effects of Dimension and Size for a Compartmental Model of Repression,* SIAM J. Appl. Math., 48 (1988), pp. 882–903.

[5] L. CERONE, B. NOVÁK, AND Z. NEUFELD, *Mathematical model for growth regulation of fission yeast* Schizosaccharomyces pombe, PLoS One (2012).

[6] F. CHANG AND S. G. MARTIN, *Shaping fission yeast with microtubules,* Cold Spring Harbor Perspect. Biol., 1 (2009) a1001347.

[7] E. J. CRAMPIN, E. A. GAFFNEY, AND P. K. MAINI, *Reaction and diffusion on growing domains: Scenarios for robust pattern formation*, Bull. Math. Biol., 61 (1999), pp 1093–1120.

[8] M. DAS, T. DRAKE, D. J. WILEY, P. BUCHWALD, D. VAVYLONIS, AND F. VERDE, *Oscillatory dynamics of Cdc42 GTPase in the control of polarized growth*, Science, 337 (2012), pp. 239–243.

[9] T. DRAKE AND D. VAVYLONIS, *Cytoskeletal dynamics in fission yeast: A review of models for polarization and division,* HFSP J., 4 (2010), pp. 122–130.

[10] J. GOU, Y.-X. LI, W. NAGATA, AND M. J. WARD, *Synchronized oscillatory dynamics for a 1-D model of membrane kinetics coupled by linear bulk diffusion,* SIAM J. Appl. Dyn. Syst., 14 (2015), pp. 2096–2137.

[11] J. Gou and M. J. Ward, *Oscillatory dynamics for a coupled membrane-bulk diffusion model with Fitzhugh-Nagumo kinetics,* SIAM J. Appl. Math., 76 (2016), pp. 776–804.

[12] S. G. Martin and F. Chang, *Dynamics of the formin for3p in actin cable assembly,* Current. Biol., 16 (2006), pp. 1161–1170.

[13] J. M. Mitchison and P. Nurse, *Growth in cell length in the fission yeast* Schizosaccharomyces pombe, J. Cell Sci., 75 (1985), pp. 357–376.

[14] B. Novak and J. J. Tyson, *Design principles of biochemical oscillators,* Nat. Rev. Mol. Cell Biol. 9 (2008) pp. 981–991.

[15] H. Wang and D. Vavylonis, *Model of for3p-mediated actin cable assembly in fission yeast,* PLoS ONE, 3 (2008), e4078.